THE ASTROPHYSICAL JOURNAL, 229:53–72, 1979 April 1

FURTHER MONITORING OF THE STRUCTURE OF SUPERLUMINAL RADIO SOURCES

G. A. SEIELSTAD, M. H. COHEN, R. P. LINFIELD, A. T. MOFFET, J. D. ROMNEY, AND R. T. SCHILIZZI*
Owens Valley Radio Observatory, California Institute of Technology
AND
D. B. SHAFFER
National Radio Astronomy Observatory, Green Bank
Received 1978 July 12; accepted 1978 October 16

ABSTRACT

We have studied the sources 3C 120, 3C 273, 3C 279, and 3C 345 at six epochs between 1975.40 and 1977.13 using very long baseline interferometry at 10.65 GHz, and at 1976.52 and 1977.41 at 5.01 GHz. The sources 3C 120 (usually) and 3C 345 (always) appear as double radio sources whose components are separating along constant position angles. Assuming their redshifts are cosmological, the *apparent* transverse velocities of separation are $v/c = 6.7 \pm 0.8$ beginning in 1966.3 ± 0.3 yr for 3C 345 and, for 3C 120, $v/c = 4.1 \pm 0.4$ beginning in 1972.4 ± 0.5 yr and continuing into 1974, then $v/c = 8.5 \pm 0.9$ beginning in 1974.4 ± 0.2 yr and continuing until mid-1976. No models of 3C 273 are derived, but evidence for superluminal expansion is presented, showing $v/c = 5.2 \pm 0.5$ beginning in 1967.6 ± 0.4 yr. Visibility functions of 3C 279 have changed very little over the period 1976.39–1977.41.

Subject headings: quasars — radio sources: variable

I. INTRODUCTION

Brightness distributions of some compact radio sources have varied so rapidly that their internal motions appear superluminal (velocities exceeding that of light) if the redshifts of the sources are of cosmological origin. The case for superluminal expansions within the sources 3C 120, 3C 273, 3C 279, and 3C 345 as of early 1976 has been reviewed by Cohen *et al.* (1977, hereafter Paper I).

The present paper extends the time base for these same four sources. We report on six very long baseline interferometry (VLBI) measurements made between 1975.40 and 1977.13 at a frequency of 10,650 MHz and on measurements made in 1976.52 and 1977.41 at 5010 MHz. The angular extents from a few of these observations have already been reported in Paper I, but this is the first presentation of the data from which these extents were determined.

The goal of these observations was to study *changes* in source structure if any occurred. We therefore sought to eliminate variations in data acquisition, processing, calibration, and interpretation by standardizing our procedures for handling each. In particular, we used the same trio of telescopes for every observation: the 40 m telescope of the Owens Valley Radio Observatory (OVRO), the 26 m telescope of the Harvard Radio Astronomy Station (HRAS), and the 43 m telescope of the National Radio Astronomy Observatory (NRAO)[1]; to these were added the 46 m telescope of the Algonquin Radio Observatory (ARO) for the 1975.40, 10,650 MHz observations and the 100 m telescope of the Max-Planck-Institut für Radioastronomie (MPIR) for the 1976.52, 5010 MHz observations.

Data from the last five epochs were all processed on the CIT–JPL VLBI processor. The first three epochs employed the NRAO processor. So far as possible, identical calibration techniques were applied to convert the raw processed data into visibility amplitudes. Finally, with but one exception, we used the same computer program to derive source models.

The result should be a higher internal consistency, permitting more valid comparisons between epochs, than in previous discussions of these radio sources.

II. OBSERVATIONS AND DATA REDUCTION

The VLBI technique has been discussed by Cohen *et al.* (1975, hereafter Paper II). Relevant baseline components and typical telescope parameters are presented there.

A detailed schedule of our observing sessions is presented in Table 1. For all 10,650 MHz observations, the telescopes accepted left circular polarization from the sky. At 5010 MHz the feeds were linearly polarized in position angle 90°.

Data were recorded with the NRAO Mark II system (Clark 1973 and Moran 1976) using a bandwidth of 2 MHz. Coherent integrations over periods from 30 seconds to 2 minutes were performed and then averaged incoherently over 8-minute intervals to produce correlation coefficients as functions of interferometer hour angle (IHA). Calibration of the

* Present address: Netherlands Foundation for Radio Astronomy, Radiosterrenwacht, Dwingeloo, The Netherlands.

[1] Operated by Associated Universities, Inc., under contract with the National Science Foundation.

TABLE 1

OBSERVING LOG

Epoch	Frequency (MHz)	Stations*
1975.40.....	10650	FOGA
1976.14.....	10650	FOG
1976.38.....	10650	FOG
1976.52.....	5010	FOGB
1976.56.....	10650	FOG
1976.73.....	10650	FOG
1977.13.....	10650	FOG
1977.41.....	5010	FOG

* F = Fort Davis (HRAS). O = Big Pine (OVRO). G = Green Bank (NRAO). A = Algonquin Park (ARO). B = Bonn (MPIR).

correlation coefficients followed the procedure outlined in Paper II. The final working data are therefore sets of correlated flux densities as functions of IHA for the various baselines, or, equivalently, as functions of U and V, the orthogonal components of the projected interferometer baselines in wavelengths.

III. RESULTS

The calibrated data are presented in Figures 1–4 for 3C 345, 5–8 for 3C 120, 9–11 for 3C 273, and 12 for 3C 279. Each vertical line has a length of 2 standard deviations and is centered on the correlated flux density measured at the given IHA. The smooth curves through these lines represent correlated flux densities calculated for the models whose parameters are summarized in Tables 2–5.

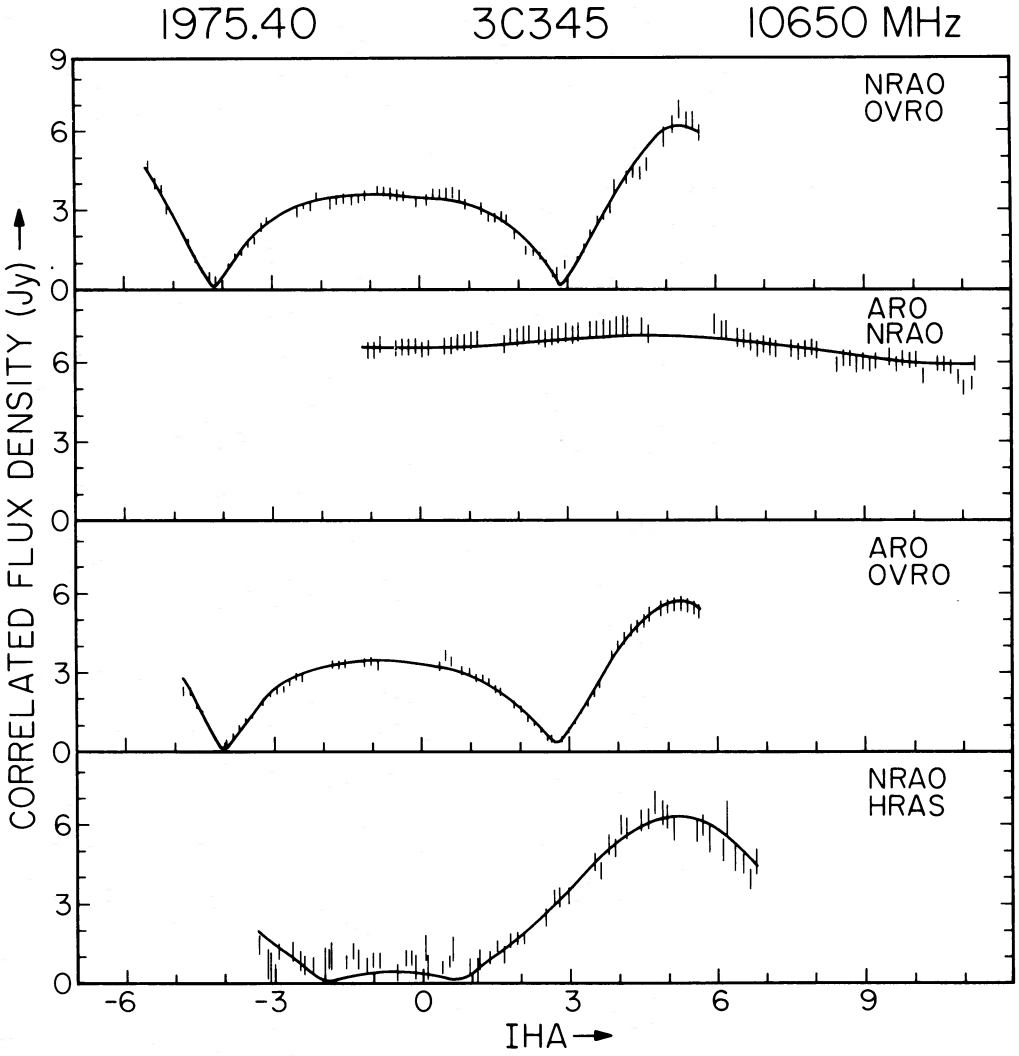

FIG. 1.—Correlated flux density versus interferometer hour angle (IHA) for 3C 345 as observed in 1975.40 at frequency 10,650 MHz over four baselines. Measurements are represented by 2 σ error bars, while the model brightness distribution with parameters listed in Table 2 yields the curves shown.

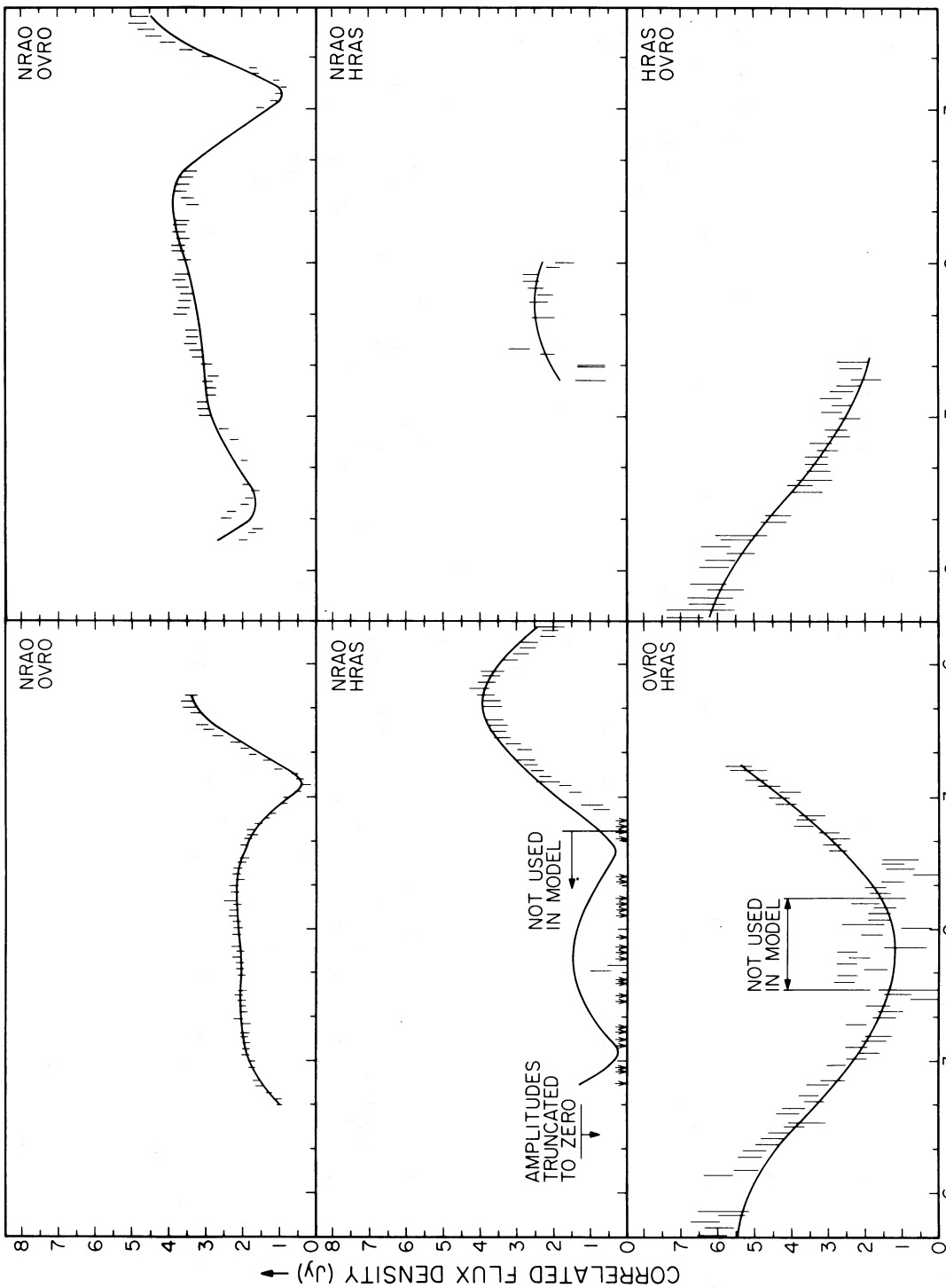

FIG. 2.—Correlated flux density versus IHA for 3C 345 as observed in 1976.38 (*left*) and 1976.56 (*right*) at 10,650 MHz over three baselines. See Table 2 for the parameters of the best-fit models (*solid curves*).

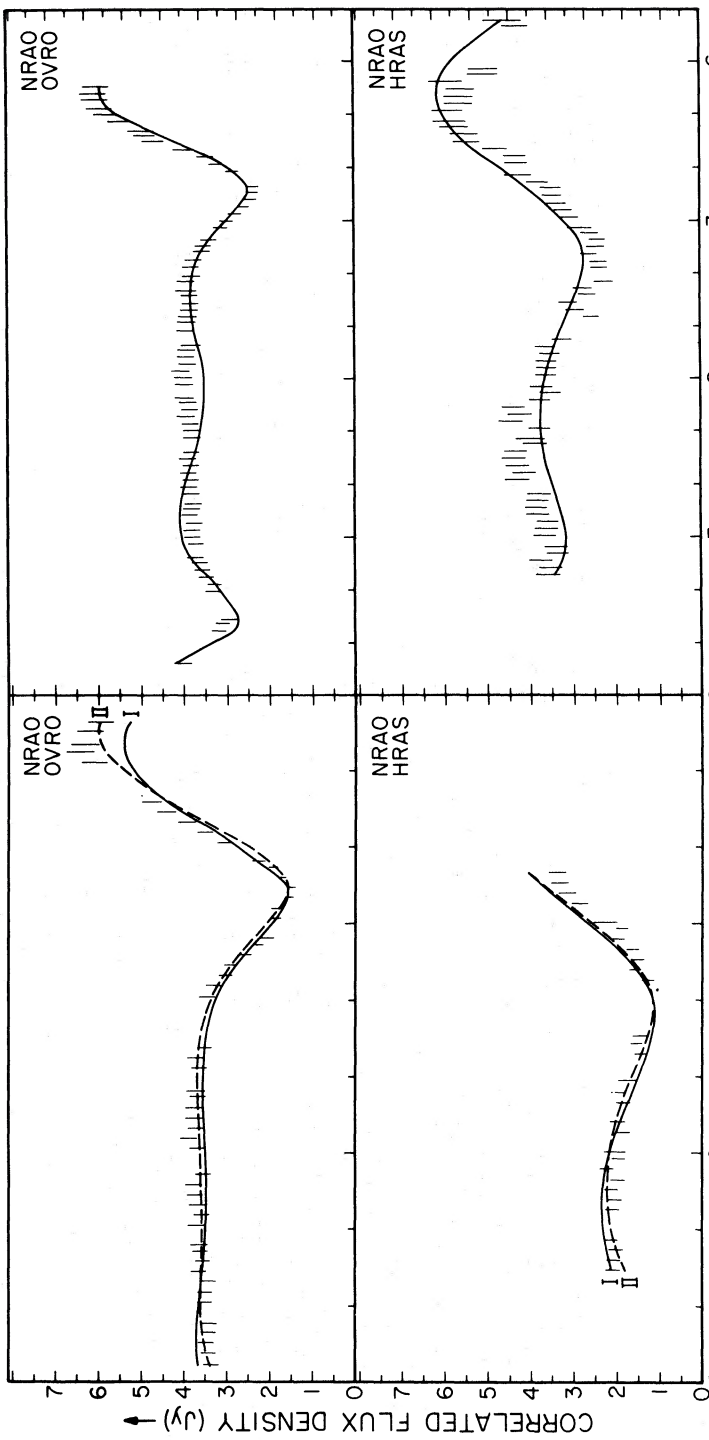

FIG. 3.—Correlated flux density versus IHA for 3C 345 as observed in 1976.73 (*left*) and 1977.13 (*right*) at 10,650 MHz over two baselines. The parameters for Model I (*solid curves*) in 1976.73 are: $(S_1 + S_2)/S_{tot} = 0.97$; $r = 1.80$ mas; $\theta = 105°3$; $S_1 = 4.82$ Jy, $\sigma_1 = 1.2$ mas, $\epsilon_1 = 0.9$, $\phi_1 = 140°$; $S_2 = 3.38$ Jy, $\sigma_2 = 0.6$ mas, $\epsilon_2 = 0.6$, $\phi_2 = 72°$. Parameters for all other models are presented in Table 2.

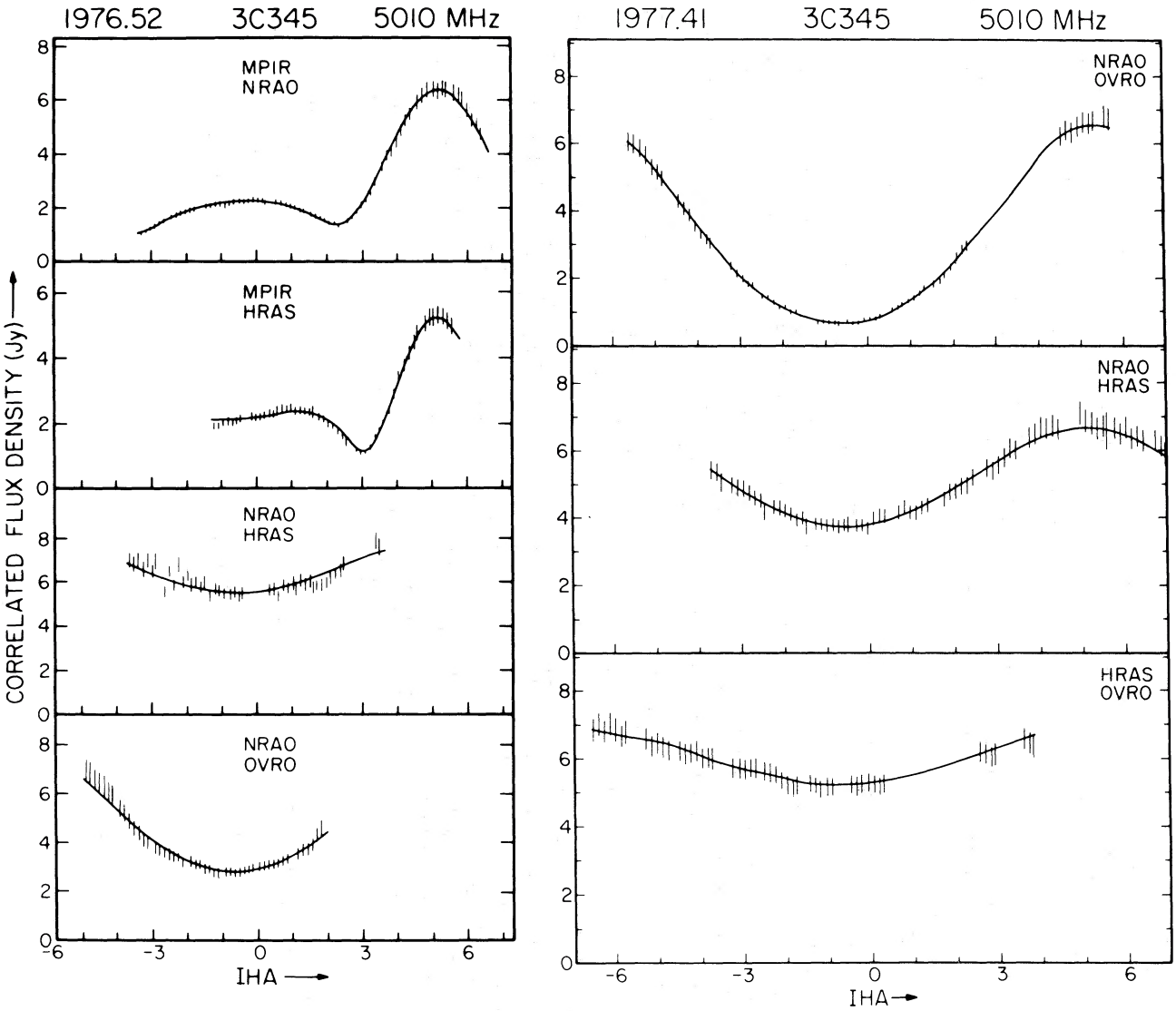

FIG. 4.—Correlated flux density versus IHA for 3C 345 as observed in 1976.52 (*left*) and 1977.41 (*right*) at 5010 MHz over three baselines. See Table 3 for the parameters of the best-fit models (*solid curves*).

TABLE 2

3C 345* (10,650 MHz)

					Stronger Component				Weaker Component			
Epoch	S_{tot}† (Jy)	$(S_1 + S_2)/S_{tot}$	r† (mas)	θ (deg)	S_1 (Jy)	σ_1 (mas)	ϵ_1	ϕ_1 (deg)	S_2 (Jy)	σ_2 (mas)	ϵ_2	ϕ_2 (deg)
1975.40.....	9.07	0.79	1.49	104.6	3.57	0.6	0.8	106	3.55	0.8	0.8	106
1976.14§.....	8.65	0.91	1.59	102.8	4.04	1.1	0.4	114	3.80	0.4	1.0	105
1976.38.....	8.89	0.80	1.71	103.5	3.92	1.2	1.0	13	3.22	1.3	0.6	161
1976.56.....	8.84	0.84	1.82	105.9	4.51	1.0	0.8	140	2.91	1.4	0.4	157
1976.73.....	8.43	1.04	1.69	100.7	5.01	1.2	0.9	139	3.76	0.7	0.6	72
1977.13.....	8.16	1.04	1.89	100.9	6.37	0.8	0.9	106	2.12	0.8	0.8	106

* The fits of these models to the data are displayed in Figs. 1–3.

† From Algonquin Radio Observatory; communicated in advance of publication by J. M. MacLeod on behalf of the group at the National Research Council of Canada.

† 1 mas ≡ 0".001.

§ Model calculated by K. I. Kellermann *et al.*, using NRAO model-fitting program.

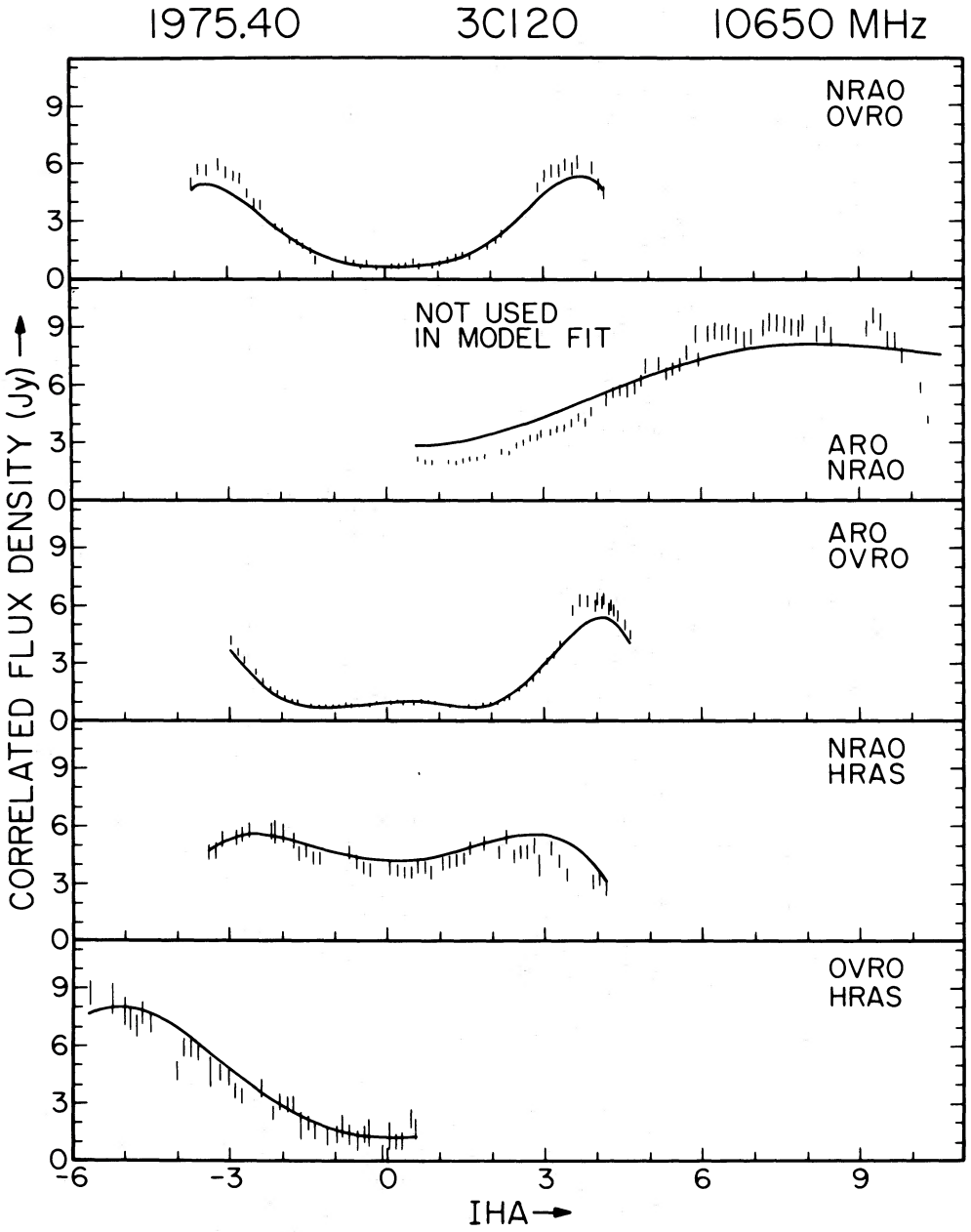

FIG. 5.—Correlated flux density versus interferometer hour angle (IHA) for 3C 120 as observed in 1975.40 at frequency 10,650 MHz over five baselines. Measurements are displayed as 2 σ error bars, while the model brightness distribution whose parameters are listed in Table 4 yields the curves shown.

TABLE 3

3C 345* (5010 MHz)

					Stronger Component				Weaker Component			
Epoch	S_{tot} (Jy)	$(S_1 + S_2)/S_{tot}$	r (mas)	θ (deg)	S_1	σ_1 (mas)	ϵ_1	ϕ_1 (deg)	S_2 (Jy)	σ_2 (mas)	ϵ_2	ϕ_2 (deg)
1976.52.....	9.1	0.90	1.50	102.7	5.85	1.3	0.5	118	2.31	0.8	0.6	130
1977.41.....	8.2	0.86	1.82	104.6	3.96	1.0	0.8	121	3.10	1.0	0.7	118

* The fits of these models to the data are displayed in Fig. 4.

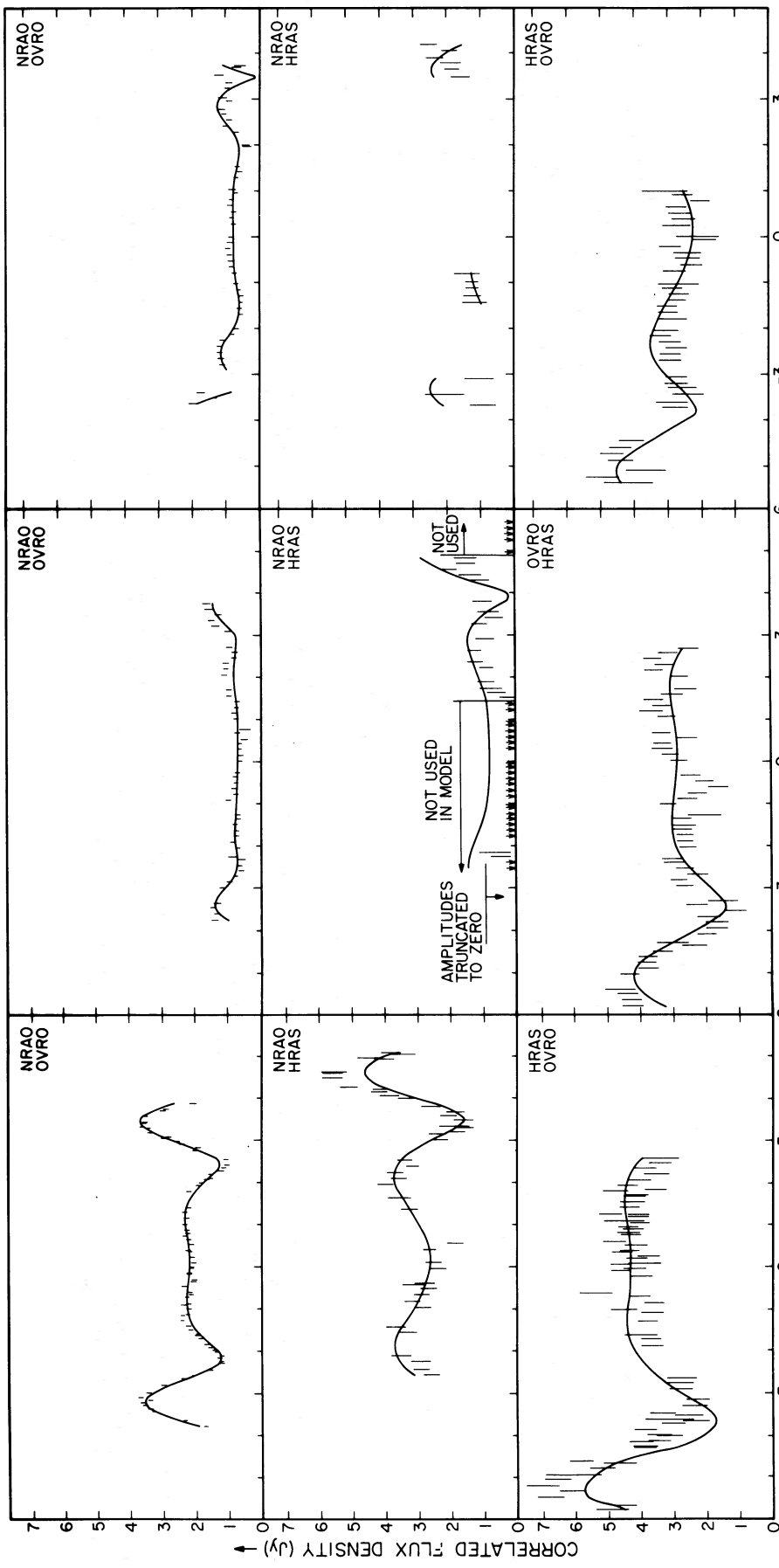

FIG. 6.—Correlated flux density versus IHA for 3C 120 as observed in 1976.13 (*left*), 1976.38 (*center*), and 1976.56 (*right*) at 10,650 MHz over three baselines. See Table 4 for the parameters of the best-fit models (*solid curves*).

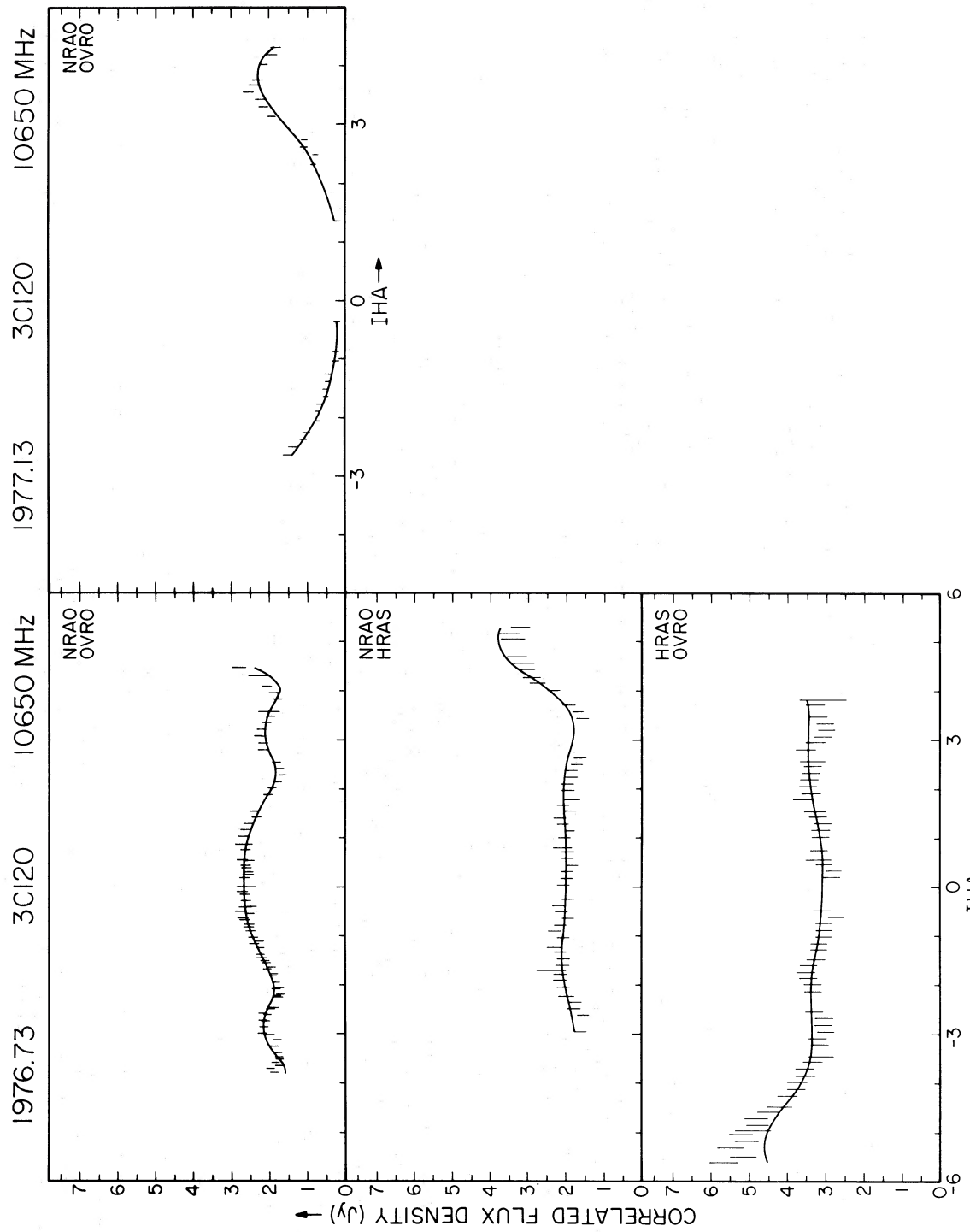

FIG. 7.—Correlated flux density versus IHA for 3C 120 as observed in 1976.73 (*left*) and 1977.13 (*right*) at 10,650 MHz over three and one baselines, respectively. See Table 4 for the parameters of the best-fit models (*solid curves*).

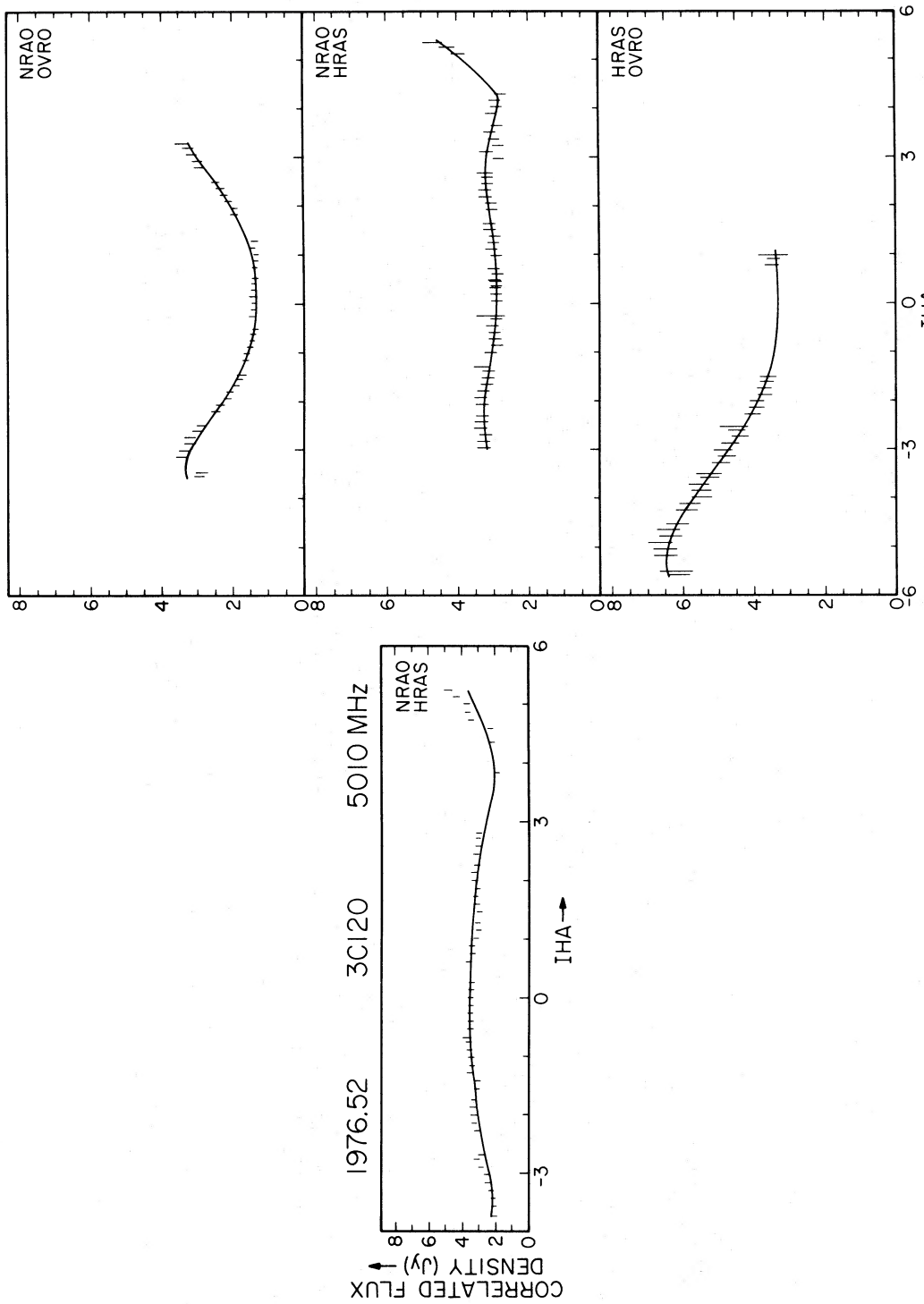

FIG. 8.—Correlated flux density versus IHA for 3C 120 as observed in 1976.52 (*left*) and 1977.41 (*right*) at 5010 MHz over one and three baselines, respectively. See Table 5 for the parameters of the best-fit models (*solid curves*).

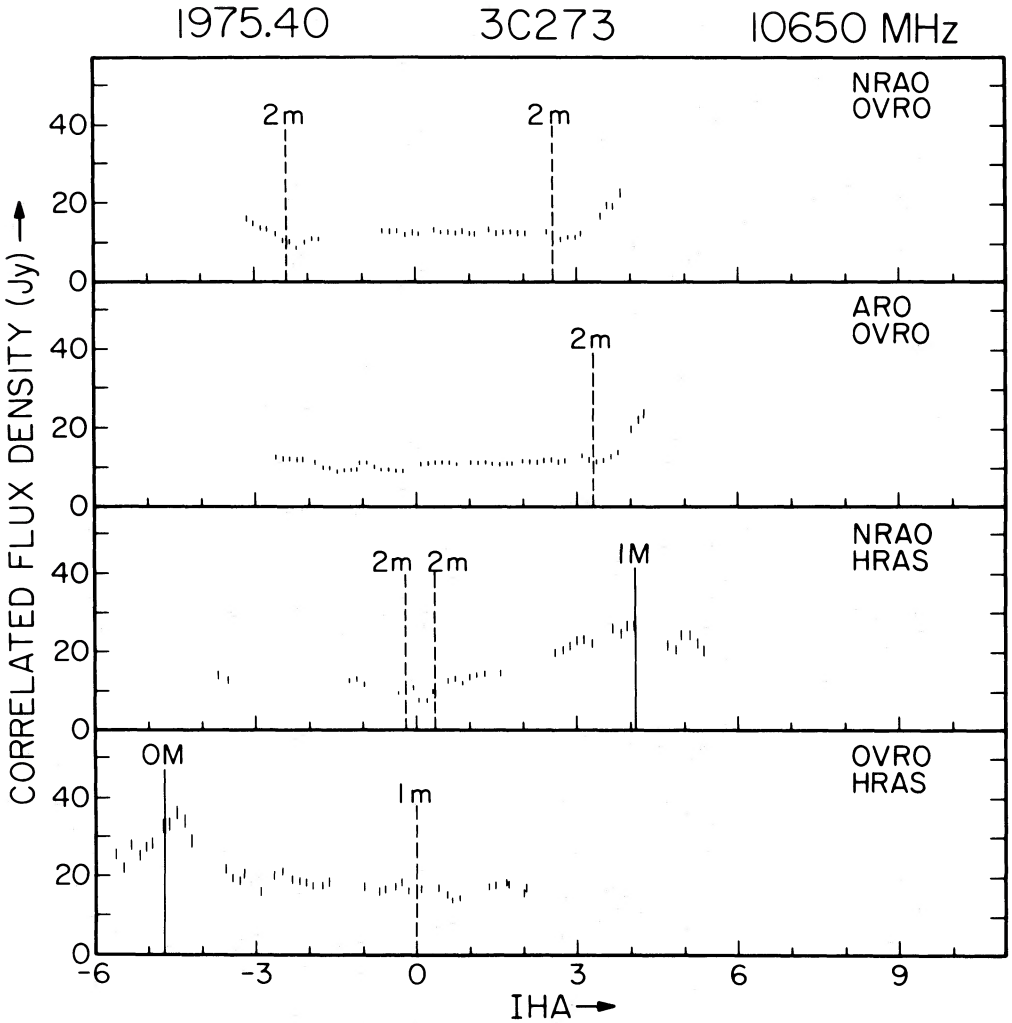

FIG. 9.—Correlated flux density versus IHA for 3C 273 as observed in 1975.40 at frequency 10,650 MHz over four baselines. Measurements are displayed as 2 σ error bars. No model fit has been attempted. The vertical lines locate maxima (M, *solid lines*) and minima (m, *dashed lines*) of the visibility data, numbered outward from the origin of the (U, V) plane.

TABLE 4

3C 120* (10,650 MHz)

					Stronger Component				Weaker Component			
Epoch	S_{tot}† (Jy)	$(S_1 + S_2)/S_{tot}$	r (mas)‡	θ (deg)	S_1 (Jy)	σ_1 (mas)	ϵ_1	ϕ_1 (deg)	S_2 (Jy)	σ_2 (mas)	ϵ_2	ϕ_2 (deg)
1975.40.....	11.3	0.75	2.84	63.4	4.79	1.0	0.9	67	3.72	1.1	1.0	67
1976.13.....	8.2	0.64	5.53	71.2	3.50	0.8	1.0	70	1.71	0.9	1.0	70
1976.38.....	7.1	0.60	6.02	65.5	3.04	2.3	0.4	62	1.24	0.7	0.8	65
1976.56.....	6.88	0.72	7.29	65.9	3.97	1.9	0.7	65	0.99	0.6	0.8	65
1976.73.....	7.14	0.65	7.03	71			TRIPLE	SOURCES§				
1977.13‖.....	6.84	0.84	2.76	67.5	3.26	1.6	0.6	65	2.48	1.3	0.6	65

* The fits of these models to the data are displayed in Figs. 5–7.

† From Algonquin Radio Observatory; communicated in advance of publication by J. M. MacLeod on behalf of the group at the National Research Council of Canada.

‡ 1 mas ≡ 0.″001.

§ Central component 3.22 Jy. Size 0.7 mas. Stronger outer component 1.10 Jy at 1.50 mas in PA 258° (78°). Size ~0.7 mas. Weaker outer component 0.34 Jy at 5.53 mas in PA 69° (249°). Size ~0.1 mas.

‖ Model based on NRAO–OVRO baseline only.

TABLE 5

3C 120* (5010 MHz)

Epoch	S_{tot} (Jy)	$(S_1 + S_2)/S_{tot}$	r (mas)	θ (deg)	S_1 (Jy)	S_2 (Jy)
1976.52†.....	8.0	0.64	4.32	66.7‡	3.76	1.34
1977.41§.....	7.5	0.93	5.24	68.4	4.38	1.30

* The fits of these models to the data are displayed in Fig. 8.

† Model based on NRAO–HRAS baseline only.

‡ Position angle fixed at this value.

§ In addition, there is a 1.32 Jy "halo," 5.5 × 4.3 mas, elongated in position angle 59°; relative location poorly determined.

In these tables, which refer to 3C 120 and 3C 345, the subscript 1 (2) refers to the stronger (weaker) of the two components. This does not imply that the same component in the sky—say, for example, the eastern—is always the stronger or always the weaker. The separation of components when a double, and of the outer components when a collinear triple, is r (milli-arcseconds). The position angle of the line of separation is θ (degrees). Flux densities are labeled S (janskys), with S_{tot} being the integrated flux density of the source. Additional parameters of individual components are their Gaussian half-power widths σ (milli-arcseconds) along their directions of maximum extent in position angle ϕ (degrees), and the ratios ϵ of their minor-to-major axes.

For 3C 273 and 3C 279 no models are calculated. For the former source, however, we present in Table 6 the distance in millions of wavelengths, measured along position angle 55°.4, from the origin to the first (s_{1m}) and the second (s_{2m}) minima in the visibility function, and to the first maximum (s_{1M}) (cf. Fig. 15). We also present $(2s_{1m})^{-1}$ in milli-arcseconds as a measure of overall source extent.

Detailed discussion of the individual sources appears in § V.

IV. UNCERTAINTIES

In the absence of phase information, model fitting is the customary means of determining source structure. This technique can only determine the optimum parameters of the model selected initially; it cannot uniquely dictate which initial model to select. This becomes particularly bothersome when, as in the case of 3C 120, a sizable fraction of the total flux is in structure too extended to be detected by our VLBI measurements. We have consistently chosen the simplest model which adequately fits the data: in cases where maxima and minima are equally spaced in the transform plane, this has been a double; where unequally spaced, a triple. When all correlated flux densities are only a small fraction of the total flux density, as in 3C 273, no detailed model is attempted.

The latitude of possible models is narrowed as the number of interferometer baselines increases. For this reason we expect the models of 3C 345 at epochs 1975.40 (10,650 MHz) and 1976.52 (5010 MHz) to be superior to the others. Conversely, when data from a single baseline only are available, the model may have little validity. This occurs for 3C 120 at 1976.52 (5010 MHz) and 1977.13 (10,650 MHz).

TABLE 6

3C 273

Epoch	s_{1m} ($10^6\lambda$)	s_{1M} ($10^6\lambda$)	s_{2m} ($10^6\lambda$)	$(2s_{1m})^{-1}$ (mas)
		10,650 MHz		
1972.33*....	59.2 ± 4.2	82.2 ± 2.9	...	1.74 ± 0.24
1972.82*....	49.6 ± 3.1	65.1 ± 0.4	85.3 ± 4.0	2.08 ± 0.26
1973.21*....	46.1 ± 2.4	61.9 ± 0.7	...	2.24 ± 0.23
1974.5†.....	38.2 ± 2.5	58.4 ± 0.5	...	2.70 ± 0.35
1975.40.....	27.8 ± 3.2	47.5 ± 3.4	79.2 ± 3.5	3.71 ± 0.84
1976.38.....	25.0 ± 1.1	...	...	4.13 ± 0.36
1976.56.....	Highly Resolved		...	...
1977.13.....	...	33.5 ± 5.0	65.0 ± 2.1	...
		5010 MHz		
1976.52.....	28.1 ± 1.2	42.1 ± 0.8	...	3.67 ± 0.16
1977.41.....	29.0 ± 1.7	39.1 ± 2.6	...	3.56 ± 0.21

* Data from Schilizzi *et al.* 1975.

† Data from Kellermann *et al.* 1977.

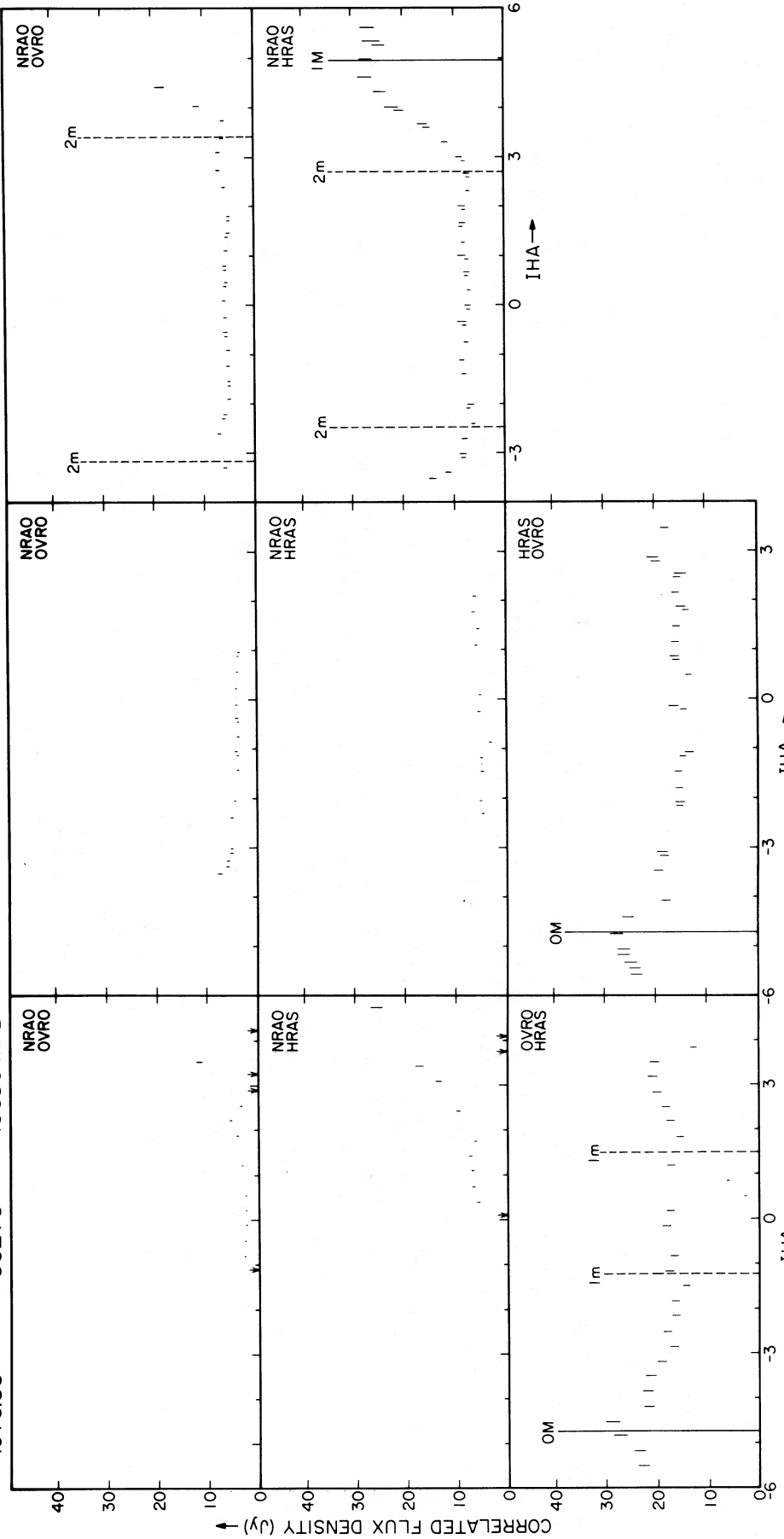

FIG. 10.—Correlated flux density versus IHA for 3C 273 as observed in 1976.38 (*left*), 1976.56 (*center*), and 1977.13 (*right*) at 10,650 MHz over the baselines indicated. The vertical lines locate maxima (M, *solid lines*) and minima (m, *dashed lines*) of the visibility data, numbered outward from the origin of the (U, V) plane.

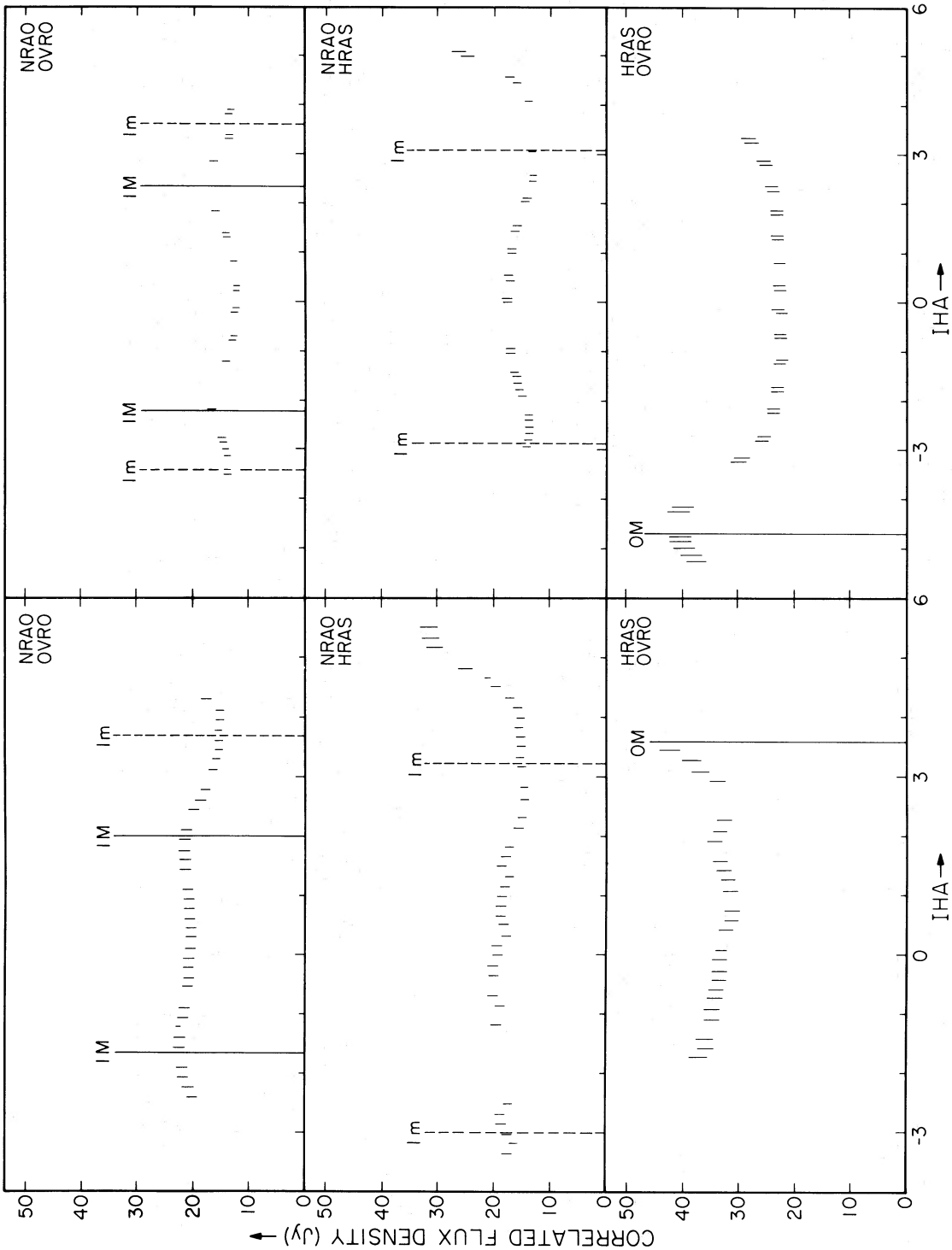

FIG. 11.—Correlated flux density versus IHA for 3C 273 as observed in 1976.52 (*left*) and 1977.41 (*right*) at 5010 MHz over three baselines. The vertical lines locate maxima (M, *solid lines*) and minima (m, *dashed lines*) of the visibility data, numbered outward from the origin of the (*U*, *V*) plane.

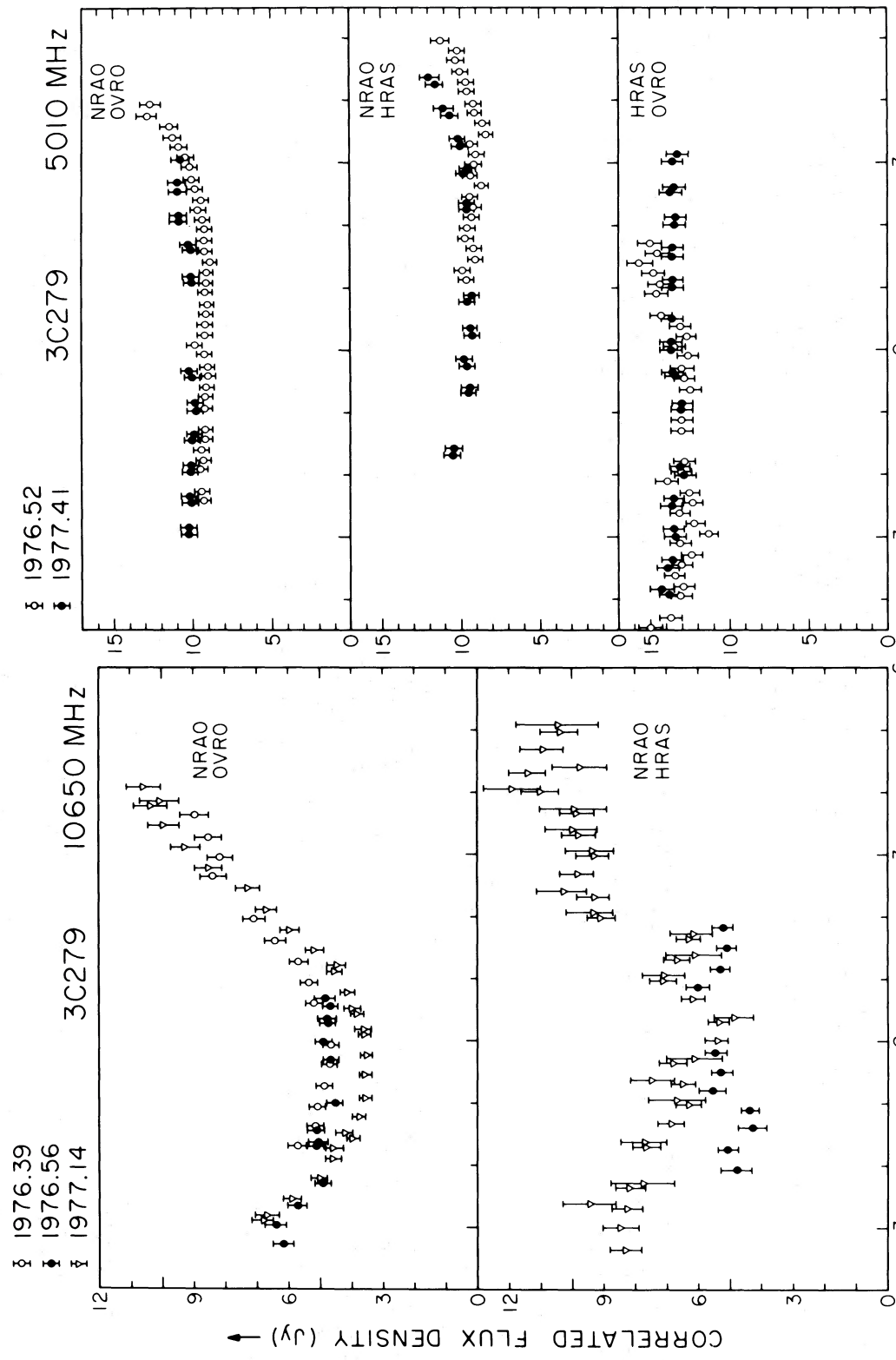

FIG. 12.—Correlated flux density versus interferometer hour angle (IHA) for 3C 279 at frequencies of 10,650 MHz (*left*) and 5010 MHz (*right*) over two and three baselines, respectively. 10,650 MHz observations were made at three epochs, and 5010 MHz observations at two.

A further well-known difficulty with model fitting is the interaction between parameters. For example, the relative flux densities of Gaussian components and their dimensions are usually strongly correlated in any fitting procedure. Formal errors do not well represent these and other correlations.

Estimates of typical errors for the parameters of 3C 120 and 3C 345 are as follows: (1) the component separation r is typically determined to ± 0.16 milliarcseconds; (2) the position angle θ of the major axis to $\pm 3°.5$; (3) the sum of the two components ($S_1 + S_2$) is accurate to perhaps $\pm 10\%$, but the individual flux densities S_1 and S_2 are less well determined, to ± 15 or 20%; (4) the size, shape, and orientation parameters (σ, ϵ, ϕ) of individual components are especially unreliable. They reveal at most only that the individual components are not point sources, that they are probably not circular in outline, and that they may not be aligned along the major axes of the sources. More explicit information should not be inferred.

V. INDIVIDUAL SOURCES

a) 3C 345

Of the four sources, we have greatest confidence in our models of 3C 345, primarily because a very large fraction of the total flux density can be accounted for by two Gaussian components. Furthermore, since the time scale for significant change appears long compared with our sampling interval, we can reliably connect successive epochs to study evolutionary behavior.

During the 2 year interval of the present study, the minima of the visibility function moved systematically closer to the origin in the (U, V) plane. We interpret this as a continuation of the increase in angular separation of the two components summarized in Paper I. Figure 13 duplicates most of the points from Figure 1 of Paper I and includes the eight points from Tables 2 and 3. The parameters of the expansion change insignificantly from the previously published values. We find from a least-squares fit of an assumed linear expansion, using all the data of Figure 13 regardless of frequency, that $d\theta/dt = (0.16 \pm 0.01)$ milli-arcsec yr^{-1} beginning from zero separation in 1966.3 $\pm$ 0.3. The corresponding apparent velocity of separation is $v/c = 6.7 \pm 0.4$ for $H_0 = 55$ km s^{-1} Mpc^{-1}, $q_0 = 0.05$, and $z = 0.595$. Our choice of a straight-line fit has no theoretical basis. The observations, however, do not demand a more complicated dependence. Some theories (e.g., Marscher 1978) predict a nonlinear relationship between separation and time.

The linearly extrapolated time of zero component separation, 1966.3, approximately coincides with a significant increase in total flux density (Paper I and Medd *et al.* 1972).

The component separation appears independent of frequency to within the measurement accuracy over the modest range of frequencies for which data are available. However, the component flux densities are frequency-dependent (cf. Tables 2 and 3). The components apparently have different and time-variable spectral indices. This has certainly been true at earlier epochs. For example, Shaffer *et al.* (1977) found different spectra for the two components in 1974.5. Furthermore, the relative 10.65 GHz flux densities of the individual components vary

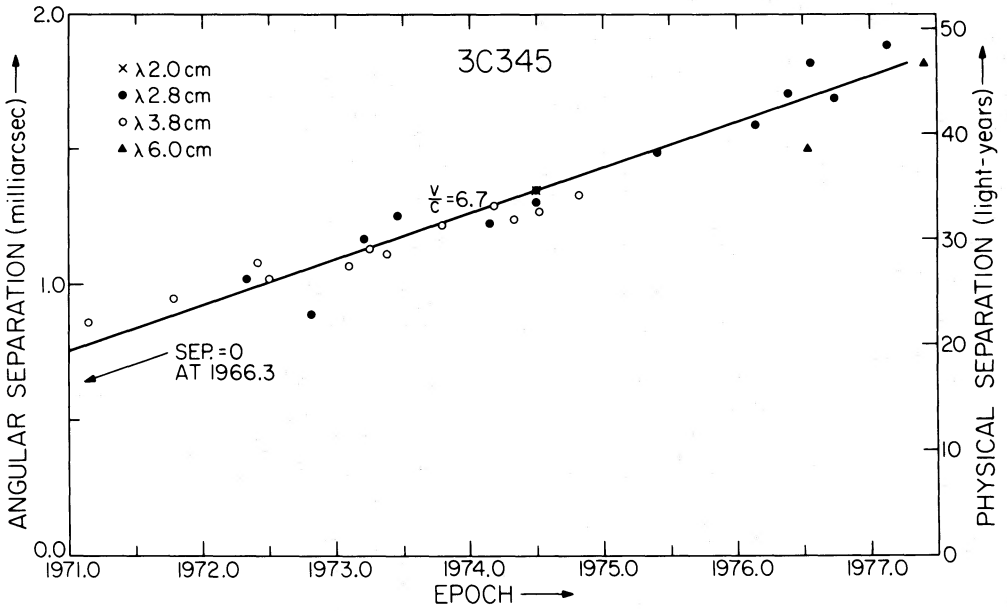

FIG. 13.—The angular separation of the two components of 3C 345 as a function of epoch. Eight values of r from Tables 2 and 3 are plotted. References to the other data points can be found in Paper I. The line is a least-squares fit to the points shown (see text for details).

systematically from near equality in 1975.40 to significant inequality in 1977.13, while at 5 GHz the trend is in the opposite sense. The total flux density, on the other hand, changes only slightly during the same interval at both frequencies. Evidently individual components may evolve more rapidly than expected from the time scales for variations in total flux density.

Shaffer *et al.* (1977) have discussed 3C 345 at epoch 1974.5 in terms of three spectral features, two of which are seen only at short wavelengths because they have standard synchrotron self-absorbed spectra. (See especially Fig. 4 of Shaffer *et al.*) The behavior described above, where the flux ratio has the opposite trend at the two frequencies, has a simple explanation in this model. Components A and B both evolve in the standard way, with their self-absorption peaks moving to lower frequencies. At 5 GHz in 1974.5 A was optically thin and B was optically thick; these evolved through 1977 when B also became optically thin. During this interval A became weaker and B stronger; they were nearly equal in 1977.41. At 10 GHz, component A was optically thin in 1974.5 and B was near the peak of its spectrum; the two had nearly equal flux densities. Evolution carried both of them well into the optically thin regime where they have unequal flux because their spectral indices are different, or because one is intrinsically stronger than the other.

This picture would be greatly strengthened if phase information were available and the component ambiguity eliminated; we could then identify the "weaker" and "stronger" components (Tables 2 and 3) at every epoch.

b) 3C 120

The source 3C 120 is by far the most rapidly variable of the four sources in both flux density (e.g., Medd *et al.* 1972) and structure (Paper I). Outbursts of flux density occur so frequently that a few components may exist simultaneously (Seielstad 1974; Aller, Olsen, and Aller 1976). The evolution of individual events is therefore confused.

As for all previous observations (Paper I and references therein), regardless of wavelength, the major axis of the brightness distribution is always within a few degrees of 65°. The mean of the measurements in Tables 4 and 5 is 67°.6.

At most epochs double-source models adequately account for the 60–90% of the flux density which has milli-arcsecond structure. The remainder of the radiation presumably occurs on a scale $\gtrsim 0.01$ arcsec. Occasionally, as in 1976.73 at 10,650 MHz and in 1977.41 at 5010 MHz the source is more complicated than a double. We have used triple-source models at these epochs, although four-component models are possible also.

After late 1976 the source appears smaller than immediately before. Similar transitions occurred in early 1972 and in mid-1974 (Paper I). These epochs may coincide with the beginnings of superluminal expansion phases. The total flux density record indeed shows major increases in early 1972 and late 1974 (Dent and Kapitzky 1976) and a small increase in mid-1976 (Dent 1977, private communication; Aller 1977, private communications).

The record of angular separations is presented in Figure 14. We have plotted the separation r for all epochs except 1976.73, where we represented the central component by the upper limit at 0.7 mas[2] and the outer pair by their separation at 7.0 mas. For the two suggested expansions, we find angular rates of 1.51 ± 0.13 and 3.12 ± 0.34 mas yr^{-1}, beginning in 1972.4 ± 0.5 and in 1974.4 ± 0.2, respectively. The corresponding apparent velocities of separation, for $z = 0.033$, are $v/c = 4.1 \pm 0.4$ and 8.5 ± 0.9. Data at all wavelengths have been used, since the separations agree to within the uncertainties. The most deviant point, from 1976.52 at 5010 MHz, is based primarily on a single minimum observed on a single baseline, and cannot therefore be considered in serious conflict, especially since a double model may seriously underestimate the complexity of the brightness distribution. The data are insufficient as yet to determine the apparent speed of a third expansion which may have begun in late 1976. Each of the expansion phases occur along the same position angle.

Lynden-Bell (1977) has suggested that throughout the entire period from early 1972 until 1975 only a single pair of components is separating about their common origin. The strengths of the several components fluctuate irregularly, so that at various times one sees (1) the two outer components, (2) the approaching component and the source at the origin, with the receding component temporarily weak, or (3) all three components simultaneously. Specific predictions were that the 3.8 cm flux density would be low at 1976.1 and that separations after 1976.1 would fall on the extrapolated dotted line of Figure 14. The former prediction is confirmed (Dent 1977, private communication), while the latter cannot be seriously challenged by our data through at least mid-1976. Later, the angular extent of the source decreased again, which, on the Lynden-Bell hypothesis, would require another simultaneous fading of the receding component and flaring of the central object. How many like occurrences can be reasonably permitted, we leave for others to judge. Particularly perplexing is how a receding component can be roughly comparable in flux density to an approaching one for some time, then disappear (or at least be overwhelmed by the briefly active central object), then reappear at again a flux density comparable to that of its original partner.

c) 3C 273

Because of its low declination ($\delta \approx 2°$) and complicated brightness distribution, models of the structure of 3C 273 have been ambiguous. For example, Legg *et al.* (1977) propose different models from those of Schilizzi *et al.* (1975) even when considering the same data. Consequently questions such as the number of source components, whether or not they are collinear,

[2] 1 mas ≡ 0".001 = 1 milliarcsecond.

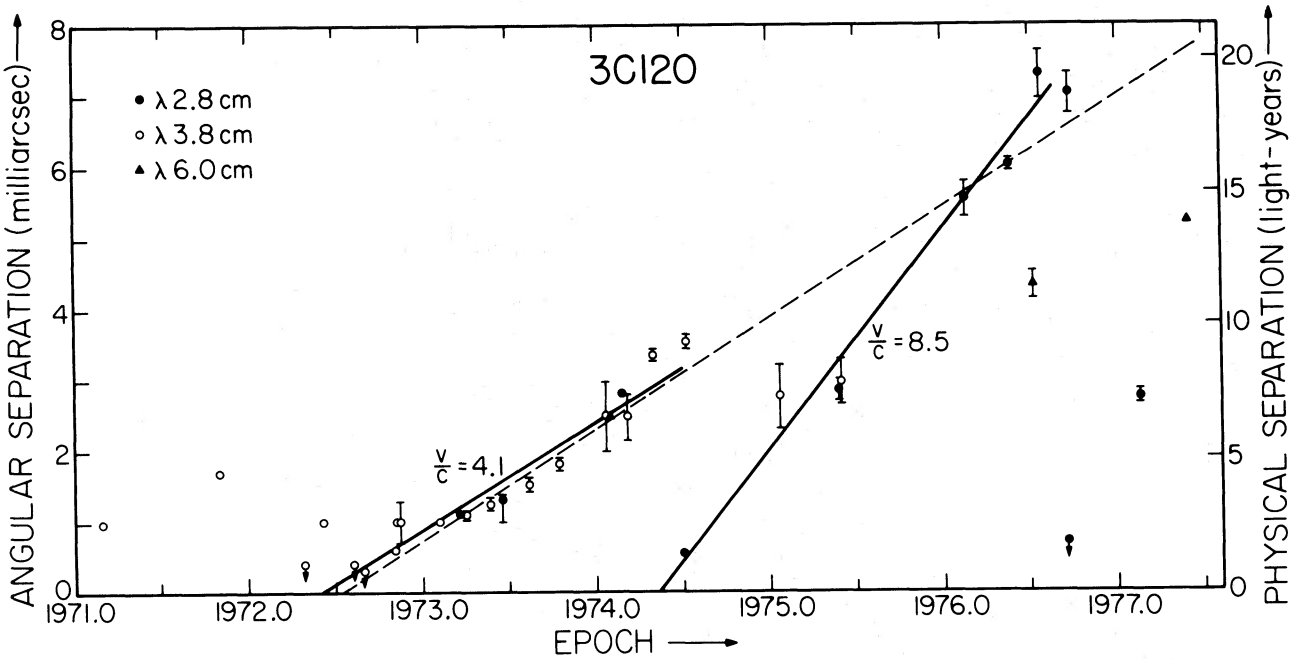

FIG. 14.—Angular separation of the outer components of 3C 120 as a function of epoch. Eight of the points are from Tables 4 and 5. References to the others can be found in Paper I. In 1976.73, an upper limit to the size of a third central component is also shown. The solid lines represent least-squares fits of the data to two phases of expansion (see text for details). The dashed line is the suggestion of Lynden-Bell (1977) for a single expansion phase.

and whether they move or are stationary have not been settled. Nor can the data displayed in Figures 9–11 hope to resolve all these ambiguities. The source is heavily resolved even on the short baselines, leaving the major structural details almost unobserved. Furthermore, the extrema are not pronounced. We therefore do not produce model brightness distributions for 3C 273. Instead we adopt the procedure used in Paper I of estimating source angular extent from the "wavelength" of the oscillations in visibility function. Long-wavelength oscillations in the (U, V) plane imply small angular sizes; short-wavelength oscillations, large sizes.

Specifically, we locate the minima (m) and the maxima (M) of the visibility curves at each epoch (Figs. 9–11). These extrema are then plotted on the (U, V) plane (Fig. 15). The so-called zeroth maximum, the one passing through the origin, occurs at the same IHA on the OVRO–HRAS baseline at every epoch (therefore the same U and V). It established an unchanging position angle for the major axis of $55° \pm 3°$. This differs slightly from previous estimates in the range 60°–68° (Cohen *et al.* 1971; Schilizzi *et al.* 1975; Kellermann *et al.* 1977). We do not consider the difference significant. It results from the highly flattened (U, V)-ellipses traced for low-declination sources and the noncollinearity of structure. The other three extrema—the first minimum (1m), first maximum(1M), and second minimum (2m)—all move systematically nearer the origin as time increases from 1972.33 to 1977.13. We interpret this change as an expansion of overall angular extent along position angle 55°.

As in Paper I, we adopt $(2s_{1m})^{-1}$ as a measure of overall angular size; this size is tabulated in Table 6 and plotted, together with other determinations, in Figure 16. The best linear fit to all these data has a slope 0.41 ± 0.04 mas yr^{-1}, corresponding for $z = 0.158$ to $v/c = 5.2 \pm 0.5$. The epoch of zero separation was 1967.6 ± 0.4 yr, near the beginning of a major increase in the source's flux density (e.g., Medd *et al.* 1972).

From Figures 15 and 16 and from Table 6 we also note the following: (i) The overall angular size of 3C 273 is independent of wavelength over the range from 2.8 to 6.0 cm. (ii) The extrema are not equally spaced. The source is therefore not a simple double. (iii) Separations between adjacent maxima and minima vary with epoch, implying that the brightness distribution does not change in a conformal way; i.e., brightness distributions at different epochs cannot be simply related by an angular scale factor.

d) 3C 279

We have far too few data on 3C 279 to derive its structure. However, we have no evidence for major changes in its brightness distribution since 1976.4 (cf. Fig. 12), although we sample infrequently. This is surprising in view of the earlier history of the source (Paper I), and doubly so because a large outburst in 7.9 GHz flux density began ca. 1975.5 and peaked ca. 1976.8 (Dent 1977, private communication). Many more data are necessary to confirm the superluminal nature of this source.

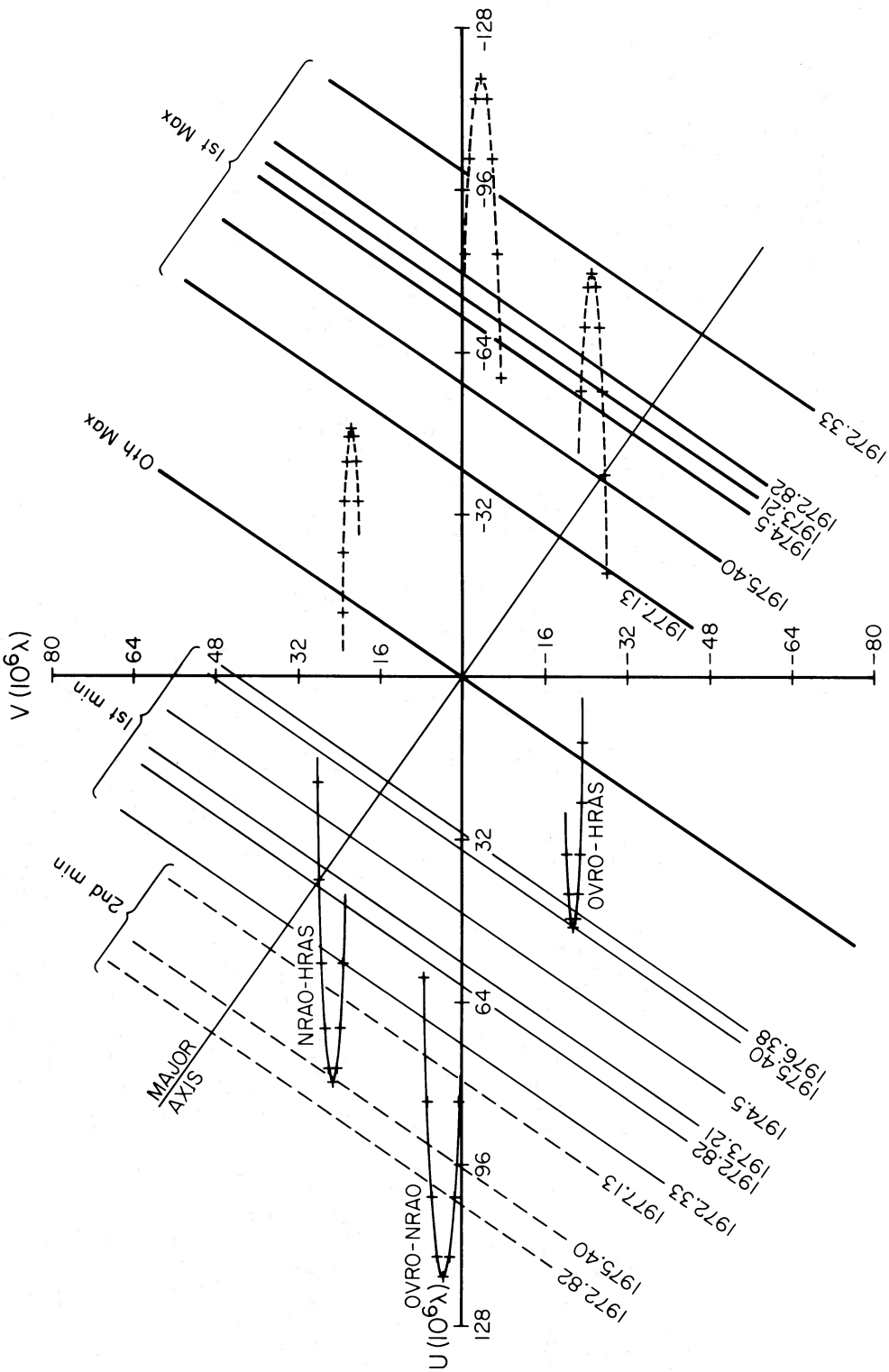

FIG. 15.—(U, V) plane coverage of 3C 273 observed with telescopes at NRAO, HRAS, and OVRO at frequency 10,650 MHz. The portions of an elliptical track (and their images mirrored through the origin) traced by each baseline vector are indicated; tick marks indicate integral hours of interferometer hour angle. The locations of the zeroth and first maxima and of the first and second minima at various epochs are also shown. Their distances from the origin along the major axis in position angle 55°.4 are listed in Table 6, together with references to the data not taken from Figs. 9 and 10.

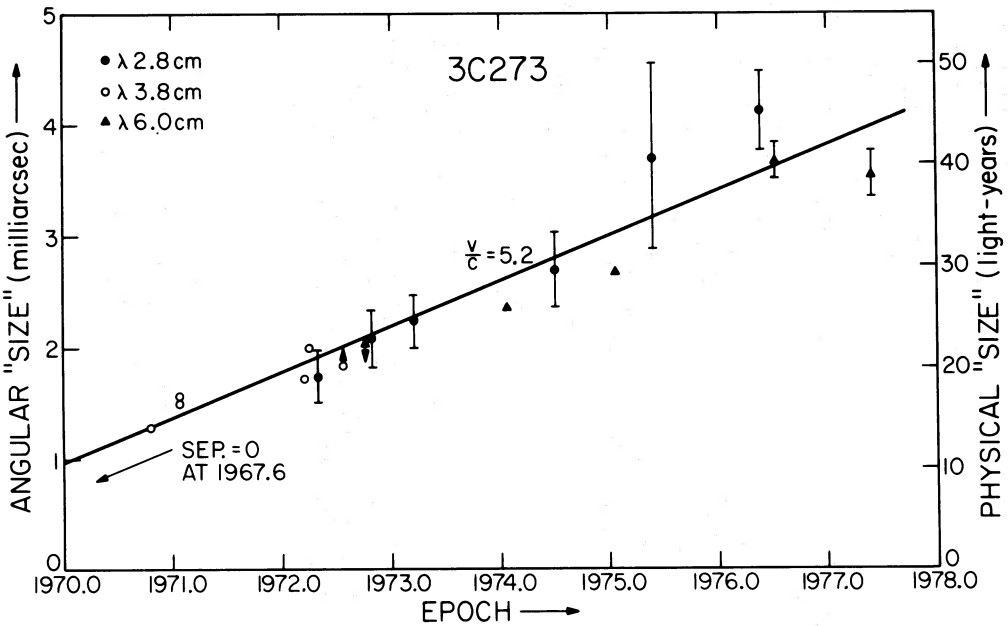

FIG. 16.—Angular size of 3C 273 as a function of epoch. The size is defined as $(2s_{1m})^{-1}$, where s_{1m} is the distance in wavelengths from the origin of the (U, V) plane to the first minimum of the visibility data (cf. Fig. 15). Six points are from Table 6. References to the others can be found in Paper I. The solid line represents a least-squares fit of all the data shown.

VI. DISCUSSION

Several theories have been proposed to account for superluminal motions (general categories are reviewed by Blandford, McKee, and Rees 1977). As yet, the brightness distribution data are not precise enough, nor the sample large enough, to critically test any of these theories. Conversely, the paucity of data has permitted theories to avoid specifics.

The proposal of Epstein and Geller (1977) is the one most seriously threatened by the data, since it predicts that the observed component separation depends upon frequency. If superluminal sources are common (see Paper I for a probability discussion), then radio-emitting objects ejected relativistically in opposite directions (Ozernoy and Sazonov 1969) are unlikely explanations, since they require special geometries of source and observer. Signals scattered, reflected, or generated in a stationary medium surrounding the active central object are more likely. Proposals requiring isotropically ejected components, of which only the few which are moving nearly along the line of sight are seen (by virtue of enhancement by relativistic beaming), founder on the constancy of position angle seen in successive outbursts. Multiple components following each other down the same approaching direction are still possible, resembling the optical jets within some galaxies.

We acknowledge with thanks receipt of data in advance of publication from H. D. Aller, W. A. Dent, K. I. Kellermann, and J. M. MacLeod. D. Sholle provided invaluable assistance with the data calibration. R. S. Simon and R. C. Walker assisted with the determination of source models. K. I. Kellermann collaborated in the early stages of this investigation and gave us the benefit of a critical reading of an early version of the manuscript. We thank J. L. Yen for his generous help with the observations at Algonquin Radio Observatory and I. I. K. Pauliny-Toth for his assistance at the Max-Planck-Institut für Radioastronomie. A. Maxwell and J. A. Ball deserve special thanks for their strenuous help at the Harvard Radio Astronomy Station. Research at the Owens Valley Radio Observatory is supported by the National Science Foundation under contract AST 77-00247. Research at the Harvard Radio Astronomy Station was supported in part by the National Science Foundation. One of the authors (G. A. S.) thanks the Departments of Astronomy and Electrical Engineering, University of Illinois at Urbana-Champaign, for their hospitality during the time when this paper was written.

REFERENCES

Aller, H. D., Olsen, E. T., and Aller, M. F. 1976, *A.J.*, **81**, 738.
Blandford, R. D., McKee, C. J., and Rees, M. J. 1977, *Nature*, **267**, 211.
Clark, B. G. 1973, *Proc. IEEE*, **61**, 1242.
Cohen, M. H., *et al.* 1977, *Nature*, **268**, 405 (Paper I).
Cohen, M. H., *et al.* 1975, *Ap. J.*, **201**, 249 (Paper II).
Cohen, M. H., Cannon, W., Purcell, G. H., Shaffer, D. B., Broderick, J. J., Kellermann, K. I., and Jauncey, D. L. 1971, *Ap. J.*, **170**, 207.
Dent, W. A., and Kapitzky, J. E. 1976, *A.J.*, **81**, 1053.
Epstein, R. I., and Geller, M. J. 1977, *Nature*, **265**, 219.
Kellermann, K. I., *et al.* 1977, *Ap. J.*, **211**, 658.
Legg, T. H., Broten, N. W., Fort, D. N., Quigley, M. J. S., Bale, F. V., Barber, P. C., and Yen, J. L. 1977, *Ap. J.*, **211**, 21.
Lynden-Bell, D. 1977, *Nature*, **270**, 396.
Marscher, A. P. 1978, *Ap. J.*, **219**, 392.
Medd, W. J., Andrew, B. H., Harvey, G. A., and Locke, J. L. 1972, *Mem. R.A.S.*, **77**, 109.

Moran, J. M. 1976, *Methods of Experimental Physics*, Vol. **12**, Part C, ed. M. L. Meeks (New York: Academic Press), pp. 174–197.
Ozernoy, L. M., and Sazonov, V. N. 1969, *Ap. Space Sci.*, **3**, 395.
Schilizzi, R. T., Cohen, M. H., Romney, J. D., Shaffer, D. B., Kellermann, K. I., Swenson, G. W., Jr., Yen, J. L., and Rinehart, R. 1975, *Ap. J.*, **201**, 263.
Seielstad, G. A. 1974, *Ap. J.*, **193**, 55.
Shaffer, D. B., *et al.* 1977, *Ap. J.*, **218**, 353.

M. H. COHEN, R. P. LINFIELD, A. T. MOFFET, and J. D. ROMNEY: Owens Valley Radio Observatory, California Institute of Technology, Mail Code 102–24, Pasadena, CA 91125

R. T. SCHILIZZI: Radiosterrenwacht Dwingeloo, Oude Hoogevensedijk 4, Dwingeloo, The Netherlands

G. A. SEIELSTAD: Owens Valley Radio Observatory, P.O. Box 387, Big Pine, CA 93513

D. B. SHAFFER: National Radio Astronomy Observatory, Green Bank, WV 24944